Rock and Soil Mechanics

Volume 44 | Issue 1 Article 7

3-13-2023

Propagation process of hydraulic fracture crossing an orthogonal discontinuity

Lei CHEN
State Key Laboratory of Petroleum Resources and Prospecting, China University of Petroleum, Beijing 102249, China

Guang-qing ZHANG
State Key Laboratory of Petroleum Resources and Prospecting, China University of Petroleum, Beijing 102249, China, zhangguangqing@cup.edu.cn

Min ZHANG
State Key Laboratory of Petroleum Resources and Prospecting, China University of Petroleum, Beijing 102249, China

Yu-jie CAO
Oil and Gas Technology Research Institute PetroChina Changqing Oilfield, Xi'an, Shaanxi 710018, China

See next page for additional authors

Custom Citation

CHEN Lei, ZHANG Guang-qing, ZHANG Min, CAO Yu-jie, SHEN Li-ji, . Propagation process of hydraulic fracture crossing an orthogonal discontinuity[J]. Rock and Soil Mechanics, 2023, 44(1): 159-170.

Propagation process of hydraulic fracture crossing an orthogonal discontinuity

Authors
Lei CHEN, Guang-qing ZHANG, Min ZHANG, Yu-jie CAO, and Li-ji SHEN

Rock and Soil Mechanics 2023 44(1): 159−170 ISSN 1000−7598
https: //doi.org/10.16285/j.rsm.2022.6041 rocksoilmech.researchcommons.org/journal

Propagation process of hydraulic fracture crossing an orthogonal discontinuity

CHEN Lei [1, 2], ZHANG Guang-qing[1, 2], ZHANG Min[1, 2], CAO Yu-jie [3], SHEN Li-ji[1, 2]

1. College of Petroleum Engineering, China University of Petroleum, Beijing 102249, China
2. State Key Laboratory of Petroleum Resources and Prospecting, China University of Petroleum, Beijing 102249, China
3. Oil and Gas Technology Research Institute PetroChina Changqing Oilfield, Xi'an, Shaanxi 710018, China

Abstract: Massive developed discontinuities are the salient geological features of unconventional oil and gas reservoirs, and the hydraulic fractures' capabilities of crossing the discontinuities concern the stimulation effects of hydraulic fracturing. To study the development of the fracture process zone (FPZ) when the hydraulic fracture orthogonally propagates through a discontinuity, the self-designed visual fracturing equipment was adopted to carry out hydraulic fracturing tests on sandstone plates with a prefabricated unbounded friction interface. Based on the digital image correlation method, the displacement and strain characteristics during the hydraulic fracture propagation across the orthogonal interface were monitored in real time. The test results show that the FPZ has developed across the interface before the hydraulic fracture extends across the interface. Whether the fracture can propagate through the interface is predetermined at the initial developmental stage of the FPZ and is not affected by the stress-softening process in the FPZ. Based on the Renshaw-Pollard criterion, a criterion considering the FPZ boundary was established for estimating the fracture propagation across the friction interface, and it was verified by test data and existing results. In comparison, the improved criterion considers a more accurate application scope of elastic fracture mechanics at the fracture front. The aspect ratio of the FPZ has a significant effect on the improved criterion, and the lower limit of friction coefficient required for the fracture propagation orthogonally across the interface declines as the aspect ratio of the FPZ rises under the same conditions.

Keywords: fracture mechanics; hydraulic fracturing; digital image correlation; geological discontinuities; fracture process zone

1 Introduction

The oil and gas reservoir is a type of sedimentary rock, and massive geological discontinuities such as natural and bedding fractures develop in the reservoir[1−2]. In the field development of oil and gas reservoirs, hydraulic fracturing is an essential initiative to promote oil and gas production. Therefore, the interaction between hydraulic fractures and geological discontinuities has traditionally been one of the focuses of rock mechanics in petroleum engineering[3−7]. In the reconstruction of shale oil and gas reservoirs, whether hydraulic fractures extend across geological discontinuities directly influences the reconstruction effect of fracturing and hence oil and gas production[6−8].

A substantial amount of research has been carried out to determine whether hydraulic fractures can travel through geological discontinuities [9−12]. Early research relied heavily on laboratory physical model tests to explore the mechanical conditions under which hydraulic fractures expand across friction interfaces[9−12]. With the advancement of numerical simulation techniques, numerical simulation methods such as the finite element method[13−14], discrete element method [15−16], and boundary element method[17] were employed to examine the mechanical behaviors of hydraulic fractures crossing the interface. Anderson[10] believed that the friction coefficient and normal stress of the interface are the dominant parameters affecting whether hydraulic fractures can cross the interface. Further research by Teufel et al.[11] discovered that, in addition to the shear strength of the interface, the horizontal minimum principal stress affects whether fractures can propagate across the interface. Based on existing findings and the linear elastic fracture mechanics, Renshaw and Pollard[18] put forward the Renshaw-Pollard criterion (R-P criterion) to determine whether fractures can orthogonally cross discontinuities. With the widespread application of the R-P criterion, new criteria for fracture propagating across the interface have recently been proposed[19−26]. For example, Gu et al.[19−20] proposed a criterion for the fracture propagating non-orthogonally across interfaces. Zhao et al.[21] established a criterion for the propagation of hydraulic fractures across the interface considering the effects of fluid-solid coupling and the related parameters. Cheng et al.[24] developed a criterion for judging the propagation of hydraulic fractures crossing the natural fracture under three-dimensional conditions, and Li et al.[25] created a criterion for identifying the hydraulic fracture with arbitrary expansion azimuth through the discontinuity.

A large number of experimental investigations have been undertaken on whether the fracture can propagate across the interface[9−12], as well as the

Received: 4 June 2022 Accepted: 16 September 2022
This work was supported by the National Science Fund for Distinguished Young Scholars (51925405) and the Strategic Cooperation Technology Projects of China National Petroleum Corporation and China University of Petroleum-Beijing (ZLZX2020-02).
First author: CHEN Lei, male, born in 1995, PhD candidate, focusing on rock elastoplastic fracture mechanics. E-mail: rawson163@163.com
Corresponding author: ZHANG Guang-qing, male, born in 1975, PhD, Professor, PhD supervisor, research interests: rock mechanics in petroleum engineering. E-mail: zhangguangqing@cup.edu.cn

theoretical research[25] and numerical simulation[13] about the linear elastic fracture process of the fracture propagating across the interface. However, less research has been conducted on the development behavior of the fracture process zone when the fracture propagates across the interface. In reality, the reservoir rock is a kind of quasi-brittle material, and a nonlinear fracture process zone (FPZ) will form at the fracture front[27−30]. The size and shape characteristics of the FPZ are related to the application range of linear elastic fracture mechanics at the fracture front[31−32], so the effect of the FPZ must be further embraced in the proper application of the R-P criterion. The monitoring exploration of the development process of the FPZ at the fracture front when the hydraulic fracture spreads across the friction interface is still missing. Although numerous factors affecting the fracture propagating across the discontinuity have been illustrated, the role of the FPZ in the fracture extending across the discontinuity is seldom considered. According to Bažant et al.[31], since the FPZ is one of the properties of rock materials, variations in its size and shape will inevitably alter the behavior of fractures crossing discontinuities.

The traditional tests about the hydraulic fracture propagation through the discontinuity were performed in the laboratory on three-dimensional rock specimens[9−12], and it is difficult to observe the fracturing process in real time. Despite the introduction of acoustic emission (AE) technology into the fracturing test[33−34] and its application to the research on the hydraulic fracture propagation across the discontinuity[35−36], there are still technical difficulties in accurately identifying the FPZ at the hydraulic fracture front using the AE technology. Building monitoring sensors (strain gauges, fiber gratings) in prefabricated specimens may be a practical approach[37], but it is difficult to precisely estimate the fracture propagation course using local monitoring points and associated limited monitoring information. In comparison, digital image correlation (DIC) is a reliable monitoring approach for obtaining whole-field deformation information, and it has been extensively utilized for the FPZ monitoring of two-dimensional specimens[27, 32, 28, 38]. However, the DIC cannot be employed to monitor the interior of three-dimensional specimens. As a result, the fracturing test in the two-dimensional plate specimen is a critical method to illustrate the FPZ when the hydraulic fracture propagates across the interface[39−40].

In this paper, hydraulic fracturing tests on two-dimensional plate specimens with prefabricated friction interfaces were performed using a self-designed visual hydraulic fracturing test apparatus. The development characteristics of the FPZ when the hydraulic fracture crosses the discontinuity were monitored by the DIC method, and the criterion of the hydraulic fracture propagation across the orthogonal discontinuity taking into account the influence of the FPZ was established, which has guidance significance for on-site hydraulic fracturing applications.

2 Visual hydraulic fracturing test

2.1 Test specimen

Sandstone specimens with artificially prefabricated friction interfaces were selected for experimental investigation to demonstrate the FPZ development process when hydraulic fractures propagate across discontinuities. As an oil and gas reservoir material, sandstone's homogeneity and isotropy are more favorable than shale's. Therefore, by employing sandstones with prefabricated interfaces, the interaction between hydraulic fractures and discontinuities can be highlighted, which helps avoid the influence of other factors and simplify research problems. Fine grained quartz sandstone from Sichuan, China, was selected for the fracturing test. The primary grain size of the sandstone is 0.12–0.25 mm, and the quartz content is up to 90% in mineral composition, followed by clay mineral. According to uniaxial compression tests, the compressive strength of the sandstone specimen is 27.04 MPa, the elastic modulus is 3.54 GPa, and the Poisson's ratio is 0.326.

The natural discontinuities were represented by the manufactured fractures. As shown in Fig. 1(a), a groove is prefabricated on the sandstone plate with dimensions of 400 mm×400 mm×50 mm, and a liquid injection support device that pressure fluid is pumped into is installed in the groove. When the pressure reaches the top, as presented in the elliptical circle in Fig. 1(a), a type I open crack will be generated on the sandstone plate. After the crack extends to the boundary and the sandstone plate is entirely broken, the fractured specimen in Fig. 1 (a) is cut along the direction of the rectangular box. As seen in Fig. 1(b), the specimen is processed to a rectangular plate with dimensions of 300 mm×250 mm×50 mm, and a circular hole is drilled in the center of the specimen to replicate the wellbore as the initiation point of hydraulic fracturing. The type I crack produced by the support device has a certain roughness and is a non-cohesive friction interface. Because the fracture is created at random, it can better simulate the natural fracture in the stratum, which provides a foundation for understanding the mechanical behaviors of hydraulic fractures crossing discontinuities.

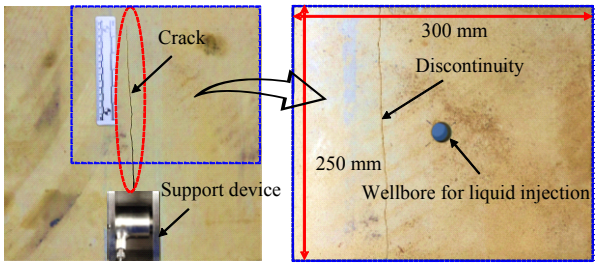

Fig. 1 Preparation of visual fracturing specimen with a discontinuity

2.2 Visual fracturing test

To address the difficulty of directly observing the extension of hydraulic fractures in traditional laboratory hydraulic fracturing tests, a two-dimensional visual hydraulic fracturing test device independently designed by China University of Petroleum (Beijing) was adopted to visually monitor the generation and extension processes of hydraulic fractures[40]. As displayed in Fig. 2(a), the visual fracturing test system consists primarily of visual fracturing equipment that can exert stress, a constant speed injection pump, a pressure gauge, an industrial camera, and light sources. The visual fracturing device is employed exclusively for the hydraulic fracturing tests on two-dimensional plate specimens, and the stress is delivered to the plate specimen through a flat jack. The top side of the specimen is mounted by a transparent acrylic cover plate through which the fracture propagation can be observed. Figure 2(b) depicts a sandstone specimen with a discontinuity placed in the visual fracturing equipment, and the hydraulic fracture will initiate and extend along the y direction when the stress is imposed on both sides of the specimen in y direction and no stress in x direction[41]. The most challenging part of the visual fracturing test is resolving the issue of fracturing fluid leakage. Since the fracturing fluid will extend to both ends of the vertical interface because the fracturing occurs in plate specimens. To prevent fracturing fluid from leaking, soft transparent tapes are pasted on both the top and bottom vertical surfaces of the specimen, as illustrated in Fig. 2(c), and the upper and lower ports of the fluid injection wellbore are sealed with epoxy resin.

During the test, the fracturing fluid was injected at a constant rate of 2 mL/min. To replicate the viscosity of the on-site fracturing fluid, the fracturing fluid is prepared from water and guar gum, accompanied by red dye. In the visual fracturing tests, 7.5 MPa stress in y direction is applied to the specimen A, and 5 MPa stress in y direction is exerted on the specimen B. A 10 MPa stress in the vertical direction is imposed on both of the specimens, while no stress is applied in x direction.

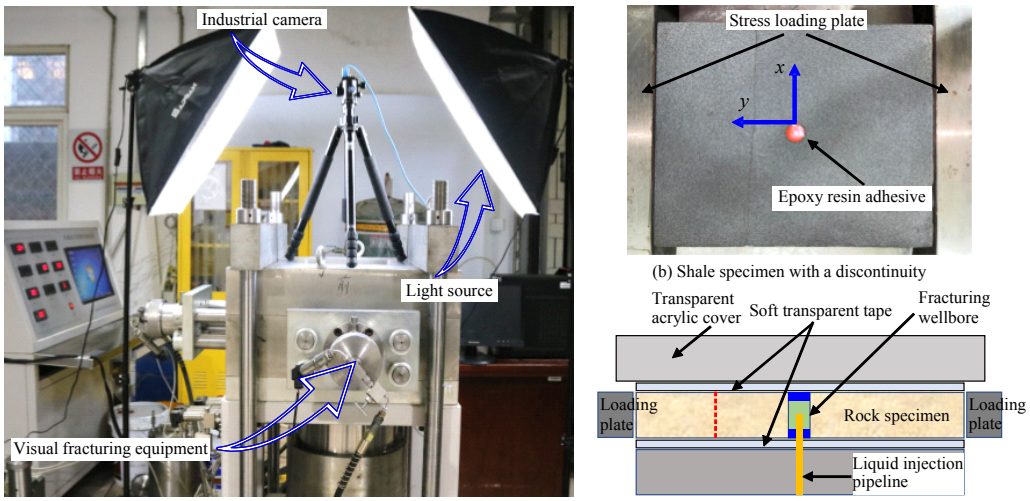

(a) Visual hydraulic fracturing test system

(c) Fracturing fluid leakage prevention method

Fig. 2 Visual fracturing device and experimental methods

2.3 DIC monitoring method

The DIC method is utilized to monitor the displacement change to accurately clarify the displacement and strain characteristics at the hydraulic fracture front during the fracture propagation. The DIC method is a non-contact measuring method[37] and has lately gained popularity in rock mechanics and fracture mechanics[42−43]. However, due to the limitation of conventional hydraulic fracturing physical model methods in the laboratory, the DIC method is seldom employed to investigate the hydraulic fracture propagation. The DIC method's primary benefit is accurately monitoring the whole field deformation information of objects, and the deformation of subsets can be tracked through the cross correlation algorithm [37, 44]. The strain field characteristics at the fracture front are required for identifying the rock fracture process zone. Based on the displacement information, the strains are characterized by the Green-Lagrange method as

$$\varepsilon_{xx}=\frac{1}{2}\left[2\frac{\partial u}{\partial x}+\left(\frac{\partial u}{\partial x}\right)^2+\left(\frac{\partial v}{\partial x}\right)^2\right] \tag{1}$$

$$\varepsilon_{yy}=\frac{1}{2}\left[2\frac{\partial v}{\partial y}+\left(\frac{\partial u}{\partial y}\right)^2+\left(\frac{\partial v}{\partial y}\right)^2\right] \tag{2}$$

where ε_{xx} and ε_{yy} are the strains in x and y directions and u, v are displacements in x, y directions.

As shown in Fig. 2(b), black and white speckles are uniformly sprayed on the specimen surface to facilitate subset distinction and identification. The industrial camera in Fig. 2(a) is employed to collect real-time photos of the fracturing process, and further DIC analysis is implemented based on the findings from Blaber et al.[44].

3 Analysis of test results

3.1 Test results

Section 2 detailed the natural interface simulation

method, visual fracturing test setup, and monitoring method. The typical pump pressure curve is plotted in Fig. 3(a). Based on the DIC monitoring results, the hydraulic fracture initiates at the red point in Fig. 3(a), and the following pressure drop reflects the hydraulic fracture expansion. The fracture initiation means the production of a new fracture rather than the start of fracture development. The fracture development is defined based on DIC strain characteristics [28, 45], and the fractures around the wellbore have developed (Figs. 3(b) and 3(e)) at the black point in Fig. 3(a). As the pumping pressure increases, the FPZ develops continuously as demonstrated in Figs. 3(e)–3(g), and the hydraulic fractures initiate and expand on both sides of the wellbore, with the propagation route following the direction of the maximum horizontal principal stress.

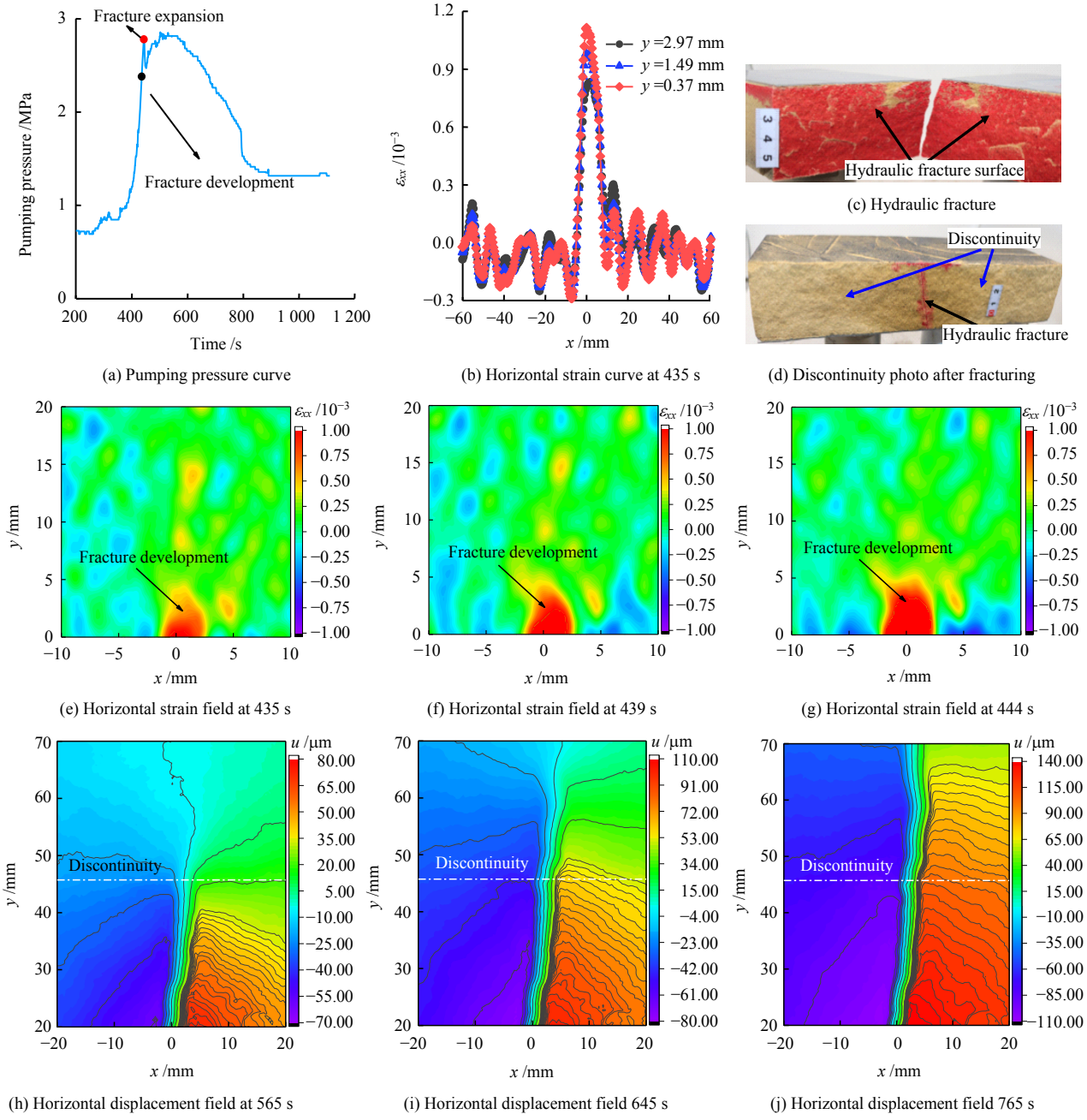

(a) Pumping pressure curve (b) Horizontal strain curve at 435 s (c) Hydraulic fracture

(d) Discontinuity photo after fracturing

(e) Horizontal strain field at 435 s (f) Horizontal strain field at 439 s (g) Horizontal strain field at 444 s

(h) Horizontal displacement field at 565 s (i) Horizontal displacement field 645 s (j) Horizontal displacement field 765 s

Fig. 3 Typical fracturing results of specimen *B*

Hydraulic fractures all spread across the discontinuity in the conducted tests, as seen in Figs. 3(h)–3(j). The hydraulic fracture surface was examined after the test, and it was found to be substantially straight in the vertical direction (Fig. 3(c)), indicating that the monitored fracture on the surface can represent the entire fracture surface. When the hydraulic fracture crosses the discontinuity, the fracturing fluid does not flow into the interface, and the fracturing fluid seepage occurs only in the limited surface area on both sides of the fracture (Fig. 3(d)), demonstrating that the interface crack does not expand appreciably. The characteristics of displacement changes near the interface before the fracture passes through the interface were analyzed based

on the test results. Figures 4(a)–4(c) show the variation characteristics of horizontal displacement in y direction near both sides of the fracture before the hydraulic fracture of specimen A crosses the discontinuity, and there is no obvious discontinuous feature in the curve near the discontinuity, demonstrating that there is no significant slip phenomenon at the interface near the fracture before the hydraulic fracture crosses the interface.

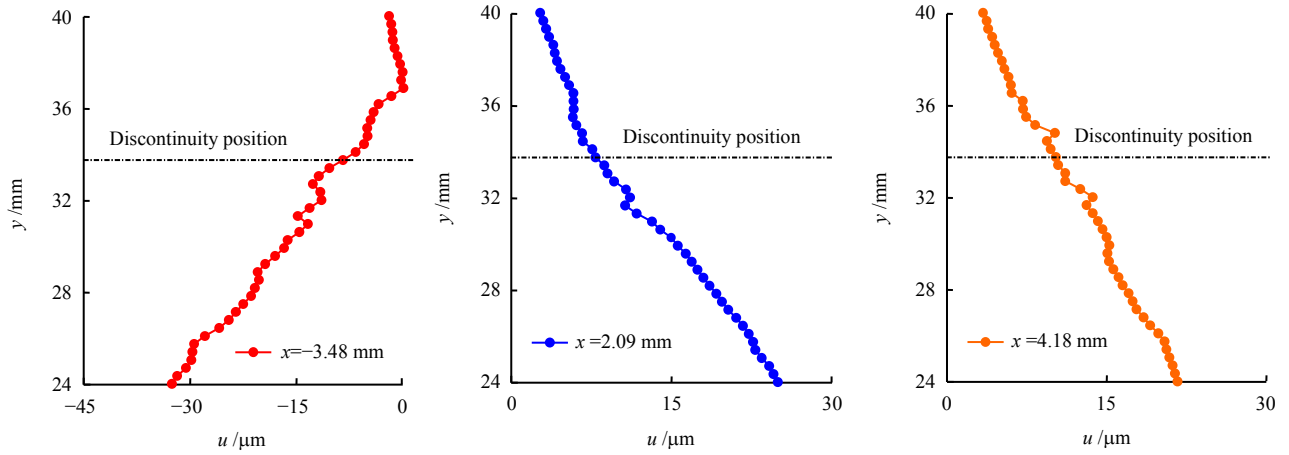

(a) $u(y)$ urve on the left side of the fracture (x=−3.48 mm) (b) $u(y)$ curve on the right side of the fracture (x=2.09 mm) (c) $u(y)$ curve on the right side of the fracture (x=4.18 mm)

Fig. 4 Variation of $u(y)$ near the fracture before fracture crosses interface (specimen A)

3.2 FPZ development

The FPZ is a nonlinear development zone at the fracture front, and it can be understood as a damage zone where microcracks accumulate in terms of damage mechanics and a tensile plastic softening zone in terms of elastoplastic mechanics[27]. The constitutive relationship of the FPZ based on the cohesion model[46] is

$$\sigma(w) = f\left(\sigma_{\mathrm{t}}, w_{\mathrm{c}}, w\right) \tag{3}$$

where w_{c} is the critical opening displacement; w is the opening displacement of the fracture in the FPZ; σ_{t} is the tensile strength; and $\sigma(w)$ is the tensile stress in the FPZ.

The tensile strain concentration at the fracture front is commonly used to represent the FPZ when the DIC method is employed[27−28, 38, 45]. However, no study has been conducted on the FPZ development process when the fracture crosses the discontinuity.

The hydraulic fracture tip position, as well as the boundary point between the non-traction tensile fracture supported by fracturing fluid and the FPZ, is required for investigating the development characteristics of the hydraulic fracture FPZ at the discontinuity, as illustrated in Fig.5(a). The current method of discussing the FPZ in three-point bending specimens based on displacement patterns[47−48] is referred to, and the change characteristics of the horizontal displacement curve are picked to define the hydraulic fracture tip. The hydraulic fracture, the FPZ, and the elastic zone are presented in Fig. 5(e). Line A represents the elastic zone, and its displacement curve shows a linear feature with a constant slope[48], as depicted in Fig. 5(b). Line B indicates the FPZ, and its displacement gradient $\partial u/\partial x$ is large in the middle and small on both sides[48], as depicted in Fig.5(c). Line D is in the displacement curve pattern at the hydraulic fracture. Due to the fracturing fluid in the hydraulic fracture, the characteristics on both sides of the fracture will show $\partial u/\partial x < 0$ under the pressure in the fracture, as depicted in Fig. 5(e), which does not occur in the conventional three-point bending test. Therefore, line C should mark the hydraulic fracture tip, and $\partial u/\partial x$ on both sides of its displacement curve is about 0, as depicted in Fig. 5(d), which suggests that there is neither compressive stress caused by the pressure in the fracture nor tensile stress required for the FPZ development on both sides. The hydraulic fracture tip is located between the hydraulic fracture and the FPZ. The horizontal displacement curves of various positions at 730 s of liquid injection loading for specimen A are given in Fig. 5(f), and the fracture growing length is estimated to be 67.55 mm based on the abovementioned pattern.

The FPZ development characteristics before the hydraulic fracture propagates through the discontinuity are observed by combining the methods of determining the hydraulic fracture tip using displacement patterns and determining the FPZ using strain concentration effects, as shown in Figs. 6(a)–6(f), where the white dotted line marks the location of the discontinuity, the black line indicates the location of the hydraulic fracture tip, and the strain concentration zone is the FPZ development zone. The FPZ does not develop to the interface when the fracture tip is distant from the discontinuity, as illustrated in Fig. 6(a). As the hydraulic fracture extends, the characteristic that the FPZ has developed across the interface before the hydraulic fracture reaches the discontinuity is commonly seen in diverse specimens, as illustrated in Figs. 6(b)–6(e). When the hydraulic fracture spreads to the discontinuity, the FPZ has developed about 10 mm across the interface, as seen in Fig. 6(f). The complete development of the FPZ across the interface indicates the emergence of a new fracture.

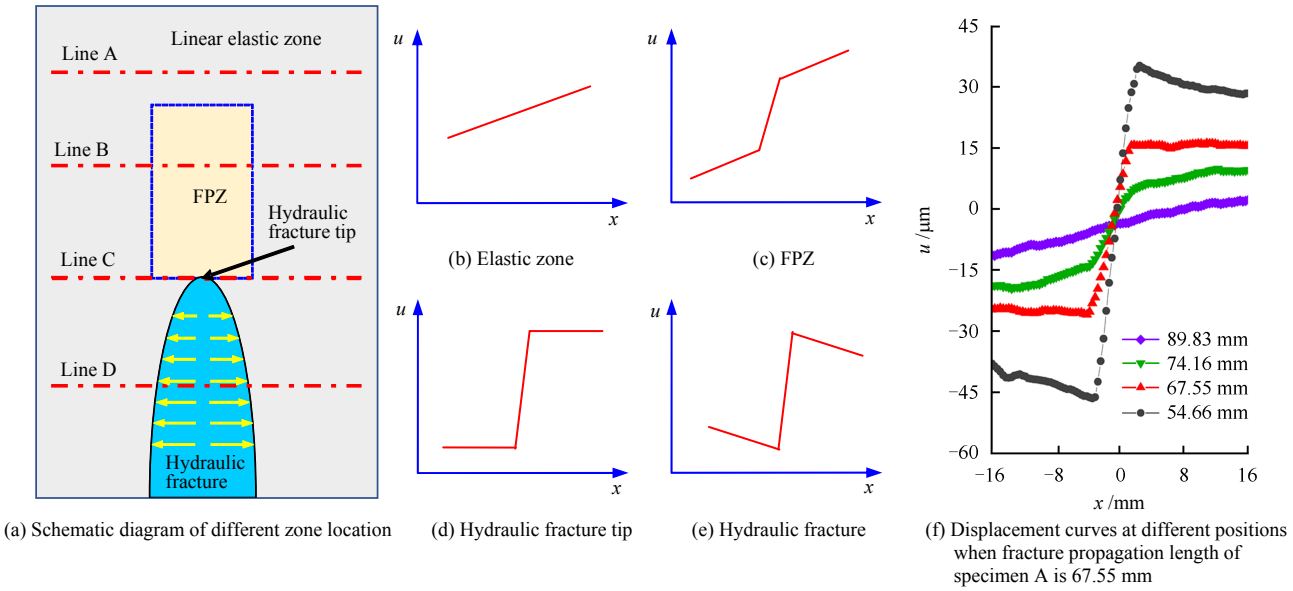

(a) Schematic diagram of different zone location (f) Displacement curves at different positions when fracture propagation length of specimen A is 67.55 mm

Fig. 5 Horizontal displacement patterns in different zones

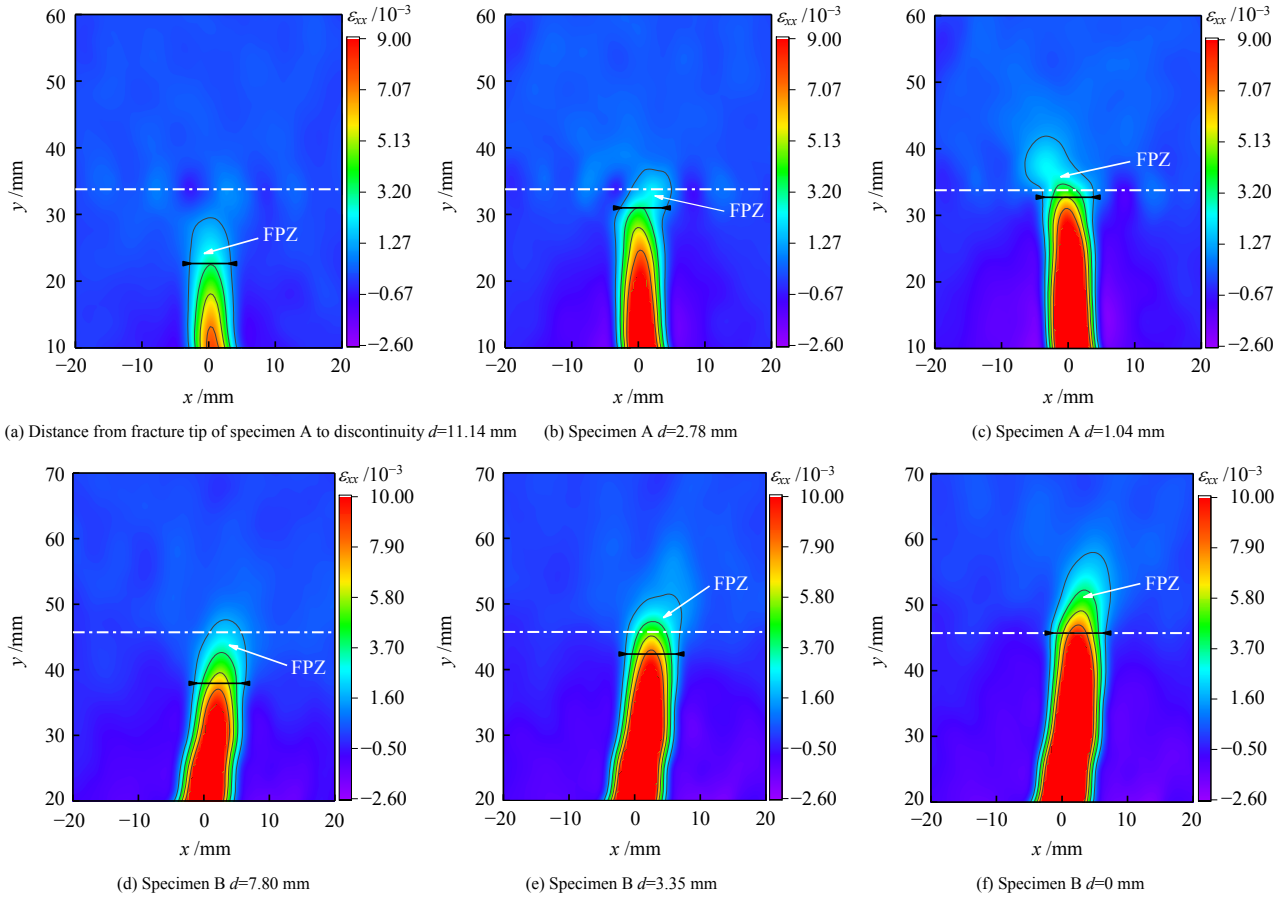

(a) Distance from fracture tip of specimen A to discontinuity d=11.14 mm (b) Specimen A d=2.78 mm (c) Specimen A d=1.04 mm

(d) Specimen B d=7.80 mm (e) Specimen B d=3.35 mm (f) Specimen B d=0 mm

Fig. 6 FPZ development before fracture crosses the discontinuity

The above test findings reveal that whether the fracture's ability to pass through the discontinuity is decided at the initial development stage of the FPZ. The impact of the FPZ at the fracture tip is often overlooked in conventional studies on the fracture propagation across the discontinuity. According to the cohesion model[46], the fracture begins to soften when the tensile strength of the rock at the fracture front reaches the tensile strength, indicating the development of the FPZ. Since the outside of the FPZ is in the linear elastic stress field, the elastic stress field outside the FPZ determines whether the hydraulic fracture can cross the discontinuity. Because the stress redistribution during the rock softening has no effect on whether the fracture can cross the interface, the R-P criterion can provide ideas for judging whether the fracture can

cross the discontinuity[18].

4 Propagation criterion considering FPZ effects

The test findings in Section 3.2 imply that the FPZ will preferentially cross the interface before the fracture passes through the discontinuity, which means that the fracture will then propagate through the interface. To prevent the impact of the singularity at the fracture tip, the R-P criteria incorporate the FPZ at its inception, and the FPZ is idealized as a circle with a radius r_{p}. The R-P criterion judges whether the fracture can pass through the interface through the maximum stress component at the friction interface, without considering the influence of the FPZ development across the interface and the FPZ difference[18]. Indeed, as the FPZ monitoring technology advances, relevant studies draw that the FPZ of rock-like quasi-brittle material often exhibits a strip shape rather than a butterfly shape or a circle calculated in theory[27−28, 45]. Based on the R-P criterion, the fundamental mechanical conditions for judging whether the fracture can travel through the interface are as follows:

$$\left.\begin{aligned}\left|\sigma_{xy}(\max)\right| < -\mu\sigma_{yy}(\max)\\ \sigma_{xx}(\max)=\sigma_{\mathrm{t}}\end{aligned}\right\} \tag{4}$$

where $\sigma_{xy}(\max)$ is the maximum shear stress of the interface; μ is the friction coefficient of the interface; $\sigma_{yy}(\max)$ is the normal stress of the interface; and $\sigma_{xx}(\max)$ is the maximum tensile stress.

Because the FPZ will preferentially cross the interface before the fracture appears as a strip shape, the R-P criterion should be improved to establish a criterion for the fracture propagation across the discontinuity considering the FPZ effects. For simplicity, the FPZ is abstracted as a rectangular region with a length l_{p} and width w_{p}, as explained in Fig.7, where $l_{\mathrm{p}}/w_{\mathrm{p}} \geqslant 1$. In addition, the materials on both sides of the discontinuity are assumed to follow the fundamental assumptions of elastic mechanics.

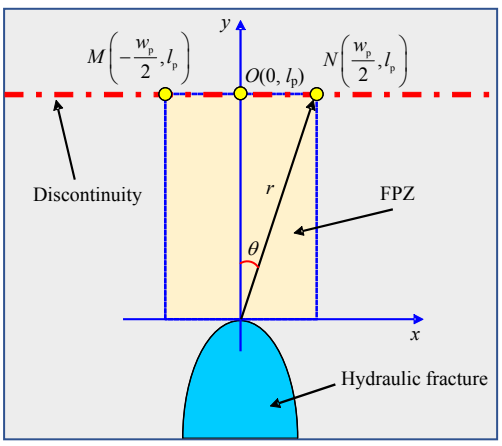

Fig. 7 FPZ at hydraulic fracture front and discontinuity

As given in Fig. 7, the actual stress field at the fracture tip is obtained by superimposing the far-field geostress and the elastic stress field at the fracture tip[18, 49]:

$$\begin{Bmatrix}\sigma_{xx}\\ \sigma_{yy}\\ \sigma_{xy}\end{Bmatrix}=\begin{Bmatrix}\sigma'_{xx}\\ \sigma'_{yy}\\ \sigma'_{xy}\end{Bmatrix}+\begin{Bmatrix}\sigma^{\mathrm{c}}_{xx}\\ \sigma^{\mathrm{c}}_{yy}\\ \sigma^{\mathrm{c}}_{xy}\end{Bmatrix}=$$

$$\begin{Bmatrix}\sigma'_{xx}\\ \sigma'_{yy}\\ \sigma'_{xy}\end{Bmatrix}+\begin{Bmatrix}\dfrac{K_{\mathrm{I}}}{\sqrt{2\pi r}}\end{Bmatrix}\begin{Bmatrix}\cos\dfrac{\theta}{2}\left(1+\sin\dfrac{\theta}{2}\sin\dfrac{3\theta}{2}\right)\\ \cos\dfrac{\theta}{2}\left(1-\sin\dfrac{\theta}{2}\sin\dfrac{3\theta}{2}\right)\\ \cos\dfrac{\theta}{2}\sin\dfrac{\theta}{2}\cos\dfrac{3\theta}{2}\end{Bmatrix} \tag{5}$$

where K_{I} is the stress intensity factor of type I crack; r and θ are polar coordinate parameters with the fracture tip as the origin; σ'_{ij} is the far-field geostress component; σ^{c}_{ij} is the elastic stress component at the fracture tip; and i, j are x, y.

The tensile stress is set to be positive, whereas the compressive stress is made to be negative. To be consistent with the test findings, the y direction is specified as the fracture propagation direction.

According to stress distribution state in the FPZ[18, 31, 46], each stress component in the FPZ is less than or equal to the stress component at the FPZ boundary, while the stress component at the FPZ boundary still conforms to the linear elastic stress solution Eq. (5). Therefore, when the top of the FPZ develops to the discontinuity, the variation characteristics of the elastic stress component at the top of the FPZ in x direction must be considered, as expressed in the following formula:

$$\begin{Bmatrix}\sigma^{\mathrm{c}}_{xx}\left(y=l_{\mathrm{p}}\right)\\ \sigma^{\mathrm{c}}_{yy}\left(y=l_{\mathrm{p}}\right)\\ \sigma^{\mathrm{c}}_{xy}\left(y=l_{\mathrm{p}}\right)\end{Bmatrix}=\begin{Bmatrix}\dfrac{K_{\mathrm{I}}}{\sqrt{2\pi l_{\mathrm{p}}/\cos\theta}}\end{Bmatrix}\begin{Bmatrix}\cos\dfrac{\theta}{2}\left(1+\sin\dfrac{\theta}{2}\sin\dfrac{3\theta}{2}\right)\\ \cos\dfrac{\theta}{2}\left(1-\sin\dfrac{\theta}{2}\sin\dfrac{3\theta}{2}\right)\\ \cos\dfrac{\theta}{2}\sin\dfrac{\theta}{2}\cos\dfrac{3\theta}{2}\end{Bmatrix} \tag{6}$$

Since $l_{\mathrm{p}}/w_{\mathrm{p}} \geqslant 1$, $|\theta| \leqslant \tan^{-1}(1/2)$ is obtained, and the change of the stress component σ^{c}_{ij} at the discontinuity from point O in Fig. 7 to point M/N is monotonous, as displayed in Figs. 8(a)–8(c).

To prevent shear slip, the shear stress on the MN surface must be smaller than the friction if the FPZ develops across the discontinuity, which is different from the R-P criteria. According to Fig. 8(a), $\left|\sigma_{xy}\right|$ at the point M/N on the interface is the largest. As seen in Fig. 8(b), the normal stress at point O on the discontinuity is the smallest when the far-field geostress σ'_{yy} is coupled. Therefore, when the stress component σ^{c}_{xy} at point M/N and the stress component σ^{c}_{yy} at point O are chosen as the judgment criteria, $\left|\sigma_{xy}\right| < -\mu\sigma_{yy}$

can be satisfied on the *MN* plane. Based on the cohesion model and the R-P criterion[18, 46], another requirement $\sigma_{xx}=\sigma_{\mathrm{t}}$ needs to be met if the FPZ continues to develop. The minimum value of σ_{xx} appears at point *O*, and the FPZ has been developed on the *MN* plane if $\sigma_{xx}=\sigma_{\mathrm{t}}$ at point *O* on the *MN* plane. Therefore, the criteria of the FPZ crossing the discontinuity can be described as

$$\begin{cases}\left|\sigma_{xy}\left(x=\pm\dfrac{w_{\mathrm{p}}}{2},y=l_{\mathrm{p}}\right)\right|<-\mu\sigma_{yy}\left(x=0,y=l_{\mathrm{p}}\right)\\ \sigma_{xx}\left(x=0,y=l_{\mathrm{p}}\right)=\sigma_{\mathrm{t}}\end{cases}\tag{7}$$

The hydraulic fracture in the real reservoir tends to expand along the direction of the maximum principal stress[41], and the far-field stress at the interface $\sigma'_{xy}=0$ [18]. As a result, the criteria of the FPZ developing across the interface can be further expressed as

$$\begin{cases}\left|\sigma^{\mathrm{c}}_{xy}\left(x=\pm\dfrac{w_{\mathrm{p}}}{2},y=l_{\mathrm{p}}\right)\right|<-\mu\left[\sigma_{\mathrm{H}}+\sigma^{\mathrm{c}}_{yy}\left(x=0,y=l_{\mathrm{p}}\right)\right]\\ \sigma_{\mathrm{h}}+\sigma^{\mathrm{c}}_{xx}\left(x=0,y=l_{\mathrm{p}}\right)=\sigma_{\mathrm{t}}\end{cases}\tag{8}$$

where σ_{H} is the maximum principal stress and σ_{h} is the minimum principal stress whose value is negative.

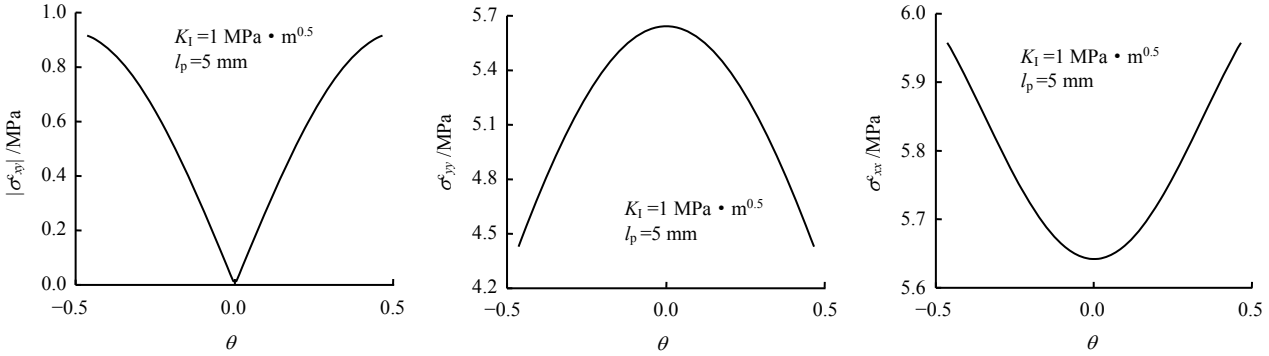

(a) Stress component $\left|\sigma^{\mathrm{c}}_{xy}\right|$ (b) Stress component σ^{c}_{yy} (c) Stress component σ^{c}_{xx}

Fig. 8 Stress component variation at the interface

When Eq. (5) is combined with Eq. (8), the criterion of the fracture propagating through the discontinuity can be further described by considering the FPZ size parameters (l_{p}, w_{p}):

$$\frac{K_{\mathrm{I}}}{\sqrt[4]{\pi^2\left(4l_{\mathrm{p}}^{\,2}+w_{\mathrm{p}}^{\,2}\right)}}\cdot\cos\frac{\tan^{-1}\left[w_{\mathrm{p}}/(2l_{\mathrm{p}})\right]}{2}\cdot\sin\frac{\tan^{-1}\left[w_{\mathrm{p}}/(2l_{\mathrm{p}})\right]}{2}\cdot\cos\frac{3\tan^{-1}\left[w_{\mathrm{p}}/(2l_{\mathrm{p}})\right]}{2}<-\mu\left(\sigma_{\mathrm{H}}+\frac{K_{\mathrm{I}}}{\sqrt{2\pi l_{\mathrm{p}}}}\right)\tag{9}$$

$$\sigma_{\mathrm{h}}+\frac{K_{\mathrm{I}}}{\sqrt{2\pi l_{\mathrm{p}}}}=\sigma_{\mathrm{t}}\tag{10}$$

When Eq. (10) is substituted into Eq. (9), the improved criterion of the fracture crossing the interface can be obtained as

$$\frac{-\sigma_{\mathrm{H}}}{\sigma_{\mathrm{t}}-\sigma_{\mathrm{h}}}>1+\frac{1}{\mu}\frac{\sqrt{l_{\mathrm{p}}}}{\sqrt[4]{l_{\mathrm{p}}^{\,2}+\dfrac{w_{\mathrm{p}}^{\,2}}{4}}}\cdot\left\{\cos\frac{\tan^{-1}\left[w_{\mathrm{p}}/(2l_{\mathrm{p}})\right]}{2}\cdot\sin\frac{\tan^{-1}\left[w_{\mathrm{p}}/(2l_{\mathrm{p}})\right]}{2}\cdot\cos\frac{3\tan^{-1}\left[w_{\mathrm{p}}/(2l_{\mathrm{p}})\right]}{2}\right\}\tag{11}$$

Furthermore, the aspect ratio of the FPZ is defined as a dimensionless parameter:

$$\frac{l_{\mathrm{p}}}{w_{\mathrm{p}}}=\lambda,\ (\lambda\geqslant 1)\tag{12}$$

Then the improved criteria can be finally expressed as

$$\frac{-\sigma_{\mathrm{H}}}{\sigma_{\mathrm{t}}-\sigma_{\mathrm{h}}}>1+\frac{1}{\mu}\cdot\frac{\sqrt{\lambda}}{\sqrt[4]{\lambda^2+0.25}}\cdot\left[\cos\frac{\tan^{-1}\left(1/2\lambda\right)}{2}\cdot\sin\frac{\tan^{-1}\left(1/2\lambda\right)}{2}\cdot\cos\frac{3\tan^{-1}\left(1/2\lambda\right)}{2}\right]\tag{13}$$

Compared with the establishment method of the R-P criterion[18], the proposed criterion of the fracture orthogonally propagating across discontinuity addresses the issue of stress singularity at the fracture tip better and can consider the influence of the FPZ shape difference. In comparison, the improved criterion can take into account the application range of linear elastic fracture mechanics at the hydraulic fracture front more precisely.

Based on the proposed criterion of the fracture orthogonally propagating across the discontinuity (Eq.

(11)), it is found that $-\sigma_H/(\sigma_t-\sigma_h)$ is always larger than 1, compared with the R-P criterion[18]:

$$\frac{-\sigma_H}{\sigma_t-\sigma_h}>\frac{0.35+0.35/\mu}{1.06} \tag{14}$$

When $\mu>0.5$, $-\sigma_H/(\sigma_t-\sigma_h)$ is less than 1, and the proposed criteria are more realistic. The fracture propagating across the discontinuity is based on the idea that the fracture propagation route must be regulated by the geostress, particularly when the geostress is considerable. $-\sigma_H/(\sigma_t-\sigma_h)<1$ suggests that the direction of the maximum principal stress has changed, so has the fracture propagation direction, and the condition that the fracture crosses the interface no longer exists.

Generally, the changing trend of the proposed criterion curve is consistent with that of the R-P criterion curve, that is, $-\sigma_H/(\sigma_t-\sigma_h)$ decreases nonlinearly as the friction coefficient increases, as presented in Fig. 9(a). However, the applicability of the improved criterion still needs to be validated with test data. The hydraulic fractures all propagate through the discontinuity in the conducted tests, which matches the prediction results of the improved criterion, as depicted in Fig. 9(a). The 20 groups of test results regarding the propagation of some fractures through the discontinuity were cited for verification[11−12, 19, 23] to further verify the reliability of the improved criterion. The improved criterion curve is plotted in Fig. 9(a) as the solid line, and the aspect ratio of the FPZ is set to 2 according to the findings on the FPZ size characteristics of rock-like materials[45]. The dotted line is the R-P criterion curve[18], and the region above the curve indicates that the fracture can cross the interface while that below the curve represents that the fracture cannot cross the interface. The data points with varied forms in Fig. 9(a) are the test data from various test results[11−12, 19, 23], among which the black data points represent that the fracture cannot cross the interface and the red data points indicate that the fracture can cross the interface. Some data points should indicate that the fracture can cross the interface based on the R-P criterion but the fracture cannot, and they can be better predicted by the improved criterion. In the cited and test data, the prediction accuracy of the improved criterion is approximately 84%, while that of the R-P criterion is about 72%, demonstrating the reliability of the improved criterion.

According to Eq. (11) and Eq. (13), the factors affecting whether the fracture crosses the discontinuity orthogonally include not only the conventional maximum and minimum principal stresses, tensile strength, and friction coefficient, but also the FPZ, especially the dimensionless parameter λ. Figure 9(b) shows the characteristics of the improved criterion curve under different λ. When the FPZ width remains unchanged, the criterion curve of the fracture crossing the discontinuity moves downward with the increase of the FPZ length, indicating the lower limit of the friction coefficient required for the fracture propagating orthogonally across the interface under the same geostress and tensile strength. In the same circumstances, the longer and narrower development shape of the hydraulic fracture FPZ may mean that the fracture is easier to cross the interface.

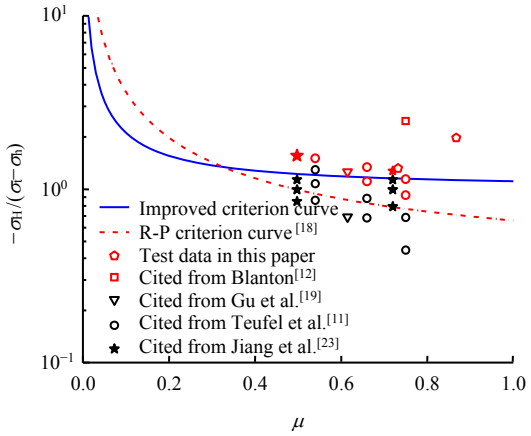

(a) Verification of improved criteria using test data

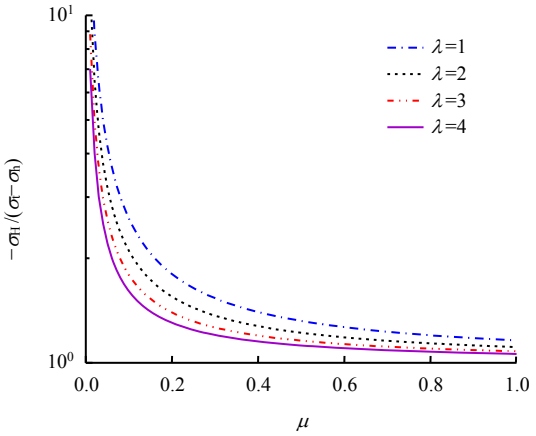

(b) Influence of FPZ aspect ratio on improved criterion

Fig. 9 Verification of the improved criterion and the influence of FPZ

5 Conclusion

The visual monitoring of hydraulic fractures can be used to explore problems that cannot be addressed in conventional hydraulic fracturing tests and help further understand the expansion mechanism of hydraulic fractures, which provides guidance for on-site hydraulic fracturing applications. The self-designed visual hydraulic fracturing test device was employed to conduct fracturing

tests on two-dimensional sandstone specimens containing discontinuities, the development characteristics of the FPZ when hydraulic fractures crossing the discontinuities were investigated, and the propagation criteria of the fracture crossing the discontinuity considering the FPZ effects was established. The primary conclusions can be summarized as follows:

(1) A visual hydraulic fracturing test technique with artificially prefabricated friction interfaces was adopted for rocks with discontinuities. The fracturing was done on plate specimens using leakage prevention measures, and the FPZ development was characterized based on the DIC monitoring method. The orthogonal propagation of the hydraulic fracture across the discontinuity was achieved, and the fracture has developed before the injection pressure reaches its maximum.

(2) The FPZ development during the fracture propagating across the discontinuity was explored, and the FPZ at the fracture front has begun to cross the interface before the hydraulic fracture does. The FPZ development directly across the interface marks the extension of subsequent hydraulic fracture across the interface, indicating that the fractures will not extend to the interface. Therefore, whether the fracture can cross the interface is determined at the initial development stage of the FPZ, and the stress redistribution in the FPZ has no effect on the behavior of the fracture crossing the interface.

(3) Based on the R-P criterion and linear elastic fracture mechanics theory, a fracture propagation criterion considering the FPZ effects was established. The improved criterion can more properly consider the application scope of linear elastic fracture mechanics at the fracture front, and its reliability was verified through the test data. The influence of the FPZ difference on the improved criterion was discussed. Under the same conditions, the lower limit of friction coefficient required for the fracture orthogonally propagating across the interface decreases as the aspect ratio of the FPZ increases.

References

[1] ZOU Cai-neng, YANG Zhi, CUI Jing-wei, et al. Formation mechanism, geological characteristics and development strategy of nonmarine shale oil in China[J]. Petroleum Exploration and Development, 2013, 40(1): 14−26.

[2] ZHONG Guan-yu, WANG Rui-he, ZHOU Wei-dong, et al. Failure characteristics of natural fracture in the vicinity of hydrofractures[J]. Rock and Soil Mechanics, 2016, 37(1): 247−255.

[3] JEFFREY R G, KEAR J, KASPERCZYK D, et al. A 2D experimental method with results for hydraulic fractures crossing discontinuities[C]//49th US Rock Mechanics/ Geomechanics Symposium. San Francisco: OnePetro, 2015.

[4] ZHAO P, GRAY K E. Analytical and machine-learning analysis of hydraulic fracture-induced natural fracture slip[J]. SPE Journal, 2021, 26(4): 1722−1738.

[5] WANG Lei, YANG Chun-he, HOU Zhen-kun, et al. Initiation and propagation of hydraulic fractures under the condition of prefabricated transverse fracture[J]. Rock and Soil Mechanics, 2016, 37(Suppl. 1): 88−94.

[6] PAN Lin-hua, CHENG Li-jun, ZHANG Shi-cheng, et al. Mechanism of fracture propagation via numerical stimulation of reservoir volume fracture in shale reservoirs[J]. Rock and Soil Mechanics, 2015, 36(1): 205−211.

[7] LLANOS E M, JEFFREY R G, HILLIS R, et al. Hydraulic fracture propagation through an orthogonal discontinuity: a laboratory, analytical and numerical study[J]. Rock Mechanics and Rock Engineering, 2017, 50(8): 2101−2118.

[8] ZHUANG Zhuo, LIU Zhan-li, WANG Tao, et al. The key mechanical problems on hydraulic fracture in shale[J]. Chinese Science Bulletin, 2016, 61(1): 72−81.

[9] DANESHY A A. Hydraulic fracture propagation in layered formations[J]. Society of Petroleum Engineers Journal, 1978, 18(1): 33−41.

[10] ANDERSON G D. Effects of friction on hydraulic fracture growth near unbonded interfaces in rocks[J]. Society of Petroleum Engineers Journal, 1981, 21(1): 21−29.

[11] TEUFEL L W, CLARK J A. Hydraulic fracture propagation in layered rock: experimental studies of fracture containment[J]. Society of Petroleum Engineers Journal, 1984, 24(1): 19−32.

[12] BLANTON T L. An experimental study of interaction between hydraulically induced and pre-existing fractures[C]//Society of Petroleum Engineers-SPE Unconventional Gas Recovery Symposium. Pittsburgh: OnePetro, 1982.

[13] LI Lian-chong, LIANG Zheng-zhao, LI Gen, et al. Three-dimensional numerical analysis of traversing and twisted fractures in hydraulic fracturing[J]. Chinese Journal of Rock Mechanics and Engineering, 2010, 29(Suppl. 1): 3208−3215.

[14] LI Jun, ZHAI Wen-bao, LIU Chao-wei, et al. Research on random propagation method of hydraulic fracture based

on zero-thickness cohesive element[J]. Rock and Soil Mechanics, 2021, 42(1): 265−279.

[15] ZHANG Feng-shou, WU Jian-fa, HUANG Hao-yong, et al. Technological parameter optimization for improving the complexity of hydraulic fractures in deep shale reservoirs[J]. Natural Gas Industry, 2021, 41(1): 125−135.

[16] ZHOU Tong, WANG Hai-bo, LI Feng-xia, et al. Numerical simulation of hydraulic fracture propagation in laminated shale reservoirs[J]. Petroleum Exploration and Development, 2020, 47(5): 1039−1051.

[17] CHEN Ming, ZHANG Shi-cheng, XU Yun, et al. Boundary element model for mechanical interaction between hydraulic fracture and natural fracture based on complementary algorithm[J]. Chinese Journal of Rock Mechanics and Engineering, 2018, 37(Suppl.2): 3947−3957.

[18] RENSHAW C E, POLLARD D D. An experimentally verified criterion for propagation across unbounded frictional interfaces in brittle, linear elastic materials[J]. International Journal of Rock Mechanics and Mining Sciences, 1995, 32(3): 237−249.

[19] GU H, WENG X, LUND J, et al. Hydraulic fracture crossing natural fracture at nonorthogonal angles: a criterion and its validation[J]. SPE Production and Operations, 2012, 27(1): 20−26.

[20] GU H, WENG X. Criterion for fractures crossing frictional interfaces at non-orthogonal angles[C]//44th US Rock Mechanics Symposium-5th US/Canada Rock Mechanics Symposium. Salt Lake City: OnePetro, 2010.

[21] ZHAO Y, HE P, ZHANG Y, et al. A new criterion for a toughness-dominated hydraulic fracture crossing a natural frictional interface[J]. Rock Mechanics and Rock Engineering, 2019, 52(8): 2617−2629.

[22] ZHU D, DU W. A criterion for a hydraulic fracture crossing a frictional interface considering T-stress[J]. Journal of Petroleum Science and Engineering, 2022, 209: 109824.

[23] JIANG Y, LIAN H, NGUYEN V P, et al. Propagation behavior of hydraulic fracture across the coal-rock interface under different interfacial friction coefficients and a new prediction model[J]. Journal of Natural Gas Science and Engineering, 2019, 68: 102894.

[24] CHENG Wan, JIN Yan, CHEN Mian, et al. A criterion for identifying hydraulic fractures crossing natural fractures in 3D space[J]. Petroleum Exploration and Development, 2014, 41(3): 336−340.

[25] LI Yong-ming, XU Wen-jun, ZHAO Jin-zhou, et al. Criteria for judging whether hydraulic fractures cross natural fractures in shale reservoirs[J]. Natural Gas Industry, 2015, 35(7): 49−54.

[26] ZHANG Ran, LI Gen-sheng, ZHAO Zhi-hong, et al. New criteria for hydraulic fracture crossing natural fractures[J]. Chinese Journal of Geotechnical Engineering, 2014, 36(3): 585−588.

[27] CHEN L, ZHANG G, ZOU Z, et al. The effect of fracture growth rate on fracture process zone development in quasi-brittle rock[J]. Engineering Fracture Mechanics, 2021, 258: 108086.

[28] PAN R, ZHANG G, LI S, et al. Influence of the fracture process zone on fracture propagation mode in layered rocks[J]. Journal of Petroleum Science and Engineering, 2021, 202: 108524.

[29] XING Y, ZHANG G, WAN B, et al. Subcritical fracturing of sandstone characterized by the acoustic emission energy[J]. Rock Mechanics and Rock Engineering, 2019, 52(7): 2459−2469.

[30] GAO Y, DONG Y, CHEN L, et al. An improved model for evaluating the brittleness of shale oil reservoirs based on dynamic elastic properties: a case study of Lucaogou formation, Jimusar Sag[J]. Geofluids, 2022, 2022: 6711977.

[31] BAŽANT Z P, PLANAS J. Fracture and size effect in concrete and other quasibrittle materials[M]. Washington D.C.: CRC Press, 1997.

[32] CHEN L, ZHANG G, ZOU Z, et al. Experimental observation of fracture process zone in sandstone from digital imaging[C]//54th U.S. Rock Mechanics/ Geomechanics Symposium. Colorado: OnePetro, 2020.

[33] XING Y, ZHANG G, LUO T, et al. Hydraulic fracturing in high-temperature granite characterized by acoustic emission[J]. Journal of Petroleum Science and Engineering, 2019, 178: 475−484.

[34] ZHOU D, ZHANG G, WANG Y, et al. Experimental investigation on fracture propagation modes in supercritical carbon dioxide fracturing using acoustic emission monitoring[J]. International Journal of Rock Mechanics and Mining Sciences, 2018, 110: 111−119.

[35] FAN Meng, JIN Yan, FU Wei-neng, et al. Experimental study on fracture propagation behavior based on acoustic emission characteristics[J]. Chinese Journal of Rock Mechanics and Engineering, 2018, 37(Suppl. 2): 3834−3841.

[36] HOU Bing, CHEN Mian, TAN Peng, et al. Monitoring of hydraulic fracture network by acoustic emission method in simulated triaxial fracturing system of shale gas reservoirs[J]. Journal of China University of Petroleum

(Edition of Natural Science), 2015, 39(1): 66−71.

[37] ZHANG G, XING Y, WANG L. Comprehensive sandstone fracturing characterization: integration of fiber Bragg grating, digital imaging correlation and acoustic emission measurements[J]. Engineering Geology, 2018, 246: 45−56.

[38] XING Y, HUANG B, NING E, et al. Quasi-static loading rate effects on fracture process zone development of mixed-mode (I-II) fractures in rock-like materials[J]. Engineering Fracture Mechanics, 2020, 240: 107365.

[39] ALTAMMAR M J, AGRAWAL S, SHARMA M M. Effect of geological layer properties on hydraulic-fracture initiation and propagation: an experimental study[J]. SPE Journal, 2019, 24(2): 757−794.

[40] CHEN L, ZHANG G, LYU Y, et al. Visualization study of hydraulic fracture propagation in unconsolidated sandstones[C]//53rd U.S. Rock Mechanics/Geomechanics Symposium. New York: OnePetro, 2019.

[41] HUBBERT M K, WILLIS D G. Mechanics of hydraulic fracturing[J]. Transactions of the AIME, 1957, 210(1): 153−168.

[42] SUN Wen-jin, JIN Ai-bing, WANG Shu-liang, et al. Study on sandstone split mechanical properties under high temperature based on the DIC technology[J]. Rock and Soil Mechanics, 2021, 42(2): 511−518.

[43] FAN Jie, ZHU Xing, HU Ju-wei, et al. Experimental study on crack propagation and damage monitoring of sandstone using three-dimensional digital image correlation technology[J]. Rock and Soil Mechanics, 2022, 43(4): 1009−1019.

[44] BLABER J, ADAIR B, ANTONIOU A. Ncorr: open-source 2D digital image correlation Matlab software[J]. Experimental Mechanics, 2015, 55(6): 1105−1122.

[45] DUTLER N, NEJATI M, VALLEY B, et al. On the link between fracture toughness, tensile strength, and fracture process zone in anisotropic rocks[J]. Engineering Fracture Mechanics, 2018, 201: 56−79.

[46] ELICES M, GUINEA G V, GÓMEZ J, et al. The cohesive zone model: advantages, limitations and challenges[J]. Engineering Fracture Mechanics, 2001, 69(2): 137−163.

[47] LIN Q, LABUZ J F. Fracture of sandstone characterized by digital image correlation[J]. International Journal of Rock Mechanics and Mining Sciences, 2013, 60: 235−245.

[48] LIN Q, WANG S, PAN P Z, et al. Imaging opening-mode fracture in sandstone under three-point bending: a direct identification of the fracture process zone and traction-free crack based on cohesive zone model[J]. International Journal of Rock Mechanics and Mining Sciences, 2020, 136: 104516.

[49] BROEK D. Elementary engineering fracture mechanics[M]. Boston: Martinus Nijhoff, 1982.